Immunologic Research (2025) 73:51
https://doi.org/10.1007/s12026-025-09603-y

RESEARCH

PANoptosis-related genes in the prognosis and immune landscape of hepatocellular carcinoma

Xiaowu Wang[1,2] · Liangchen Qu[2] · Zhikai Wen[1,3] · Zhixuan Wu[3] · Yuxiang Xue[1] · Xuejia Yang[3] · Ziwei Yuan[3] · Yangyang Guo[2,4] · Xingcheng Lin[1]

Received: 21 April 2024 / Accepted: 4 February 2025

Abstract

In hepatocellular carcinoma (HCC) individuals, the influence of numerous variables on the HCC prognosis has gained widespread recognition. Nevertheless, there remains a need for further elucidation regarding the underlying mechanism of PANoptosis-related genes (PRGs) on HCC. A consensus clustering approach, based on the TCGA-LIHC data, was used to identify specific subtypes linked to PANoptosis in this study. Next, a signature consisting of predictive differentially expressed genes for these subtypes was established using a least absolute shrinkage and selection operator (LASSO) regression analysis. Additionally, the reliability of the signature was confirmed through verification investigations using the data from the ICGC database and TCGA-LIHC. In the end, we developed a nomogram to enhance the clinical effectiveness of our prediction tool. PRG signature in this study has been highly related to the prognosis of individuals diagnosed with HCC, which was established with six genes. Also, this signature and clinicopathological features were put together to create a nomogram. Interestingly, the forecasting efficiency of this combination approach is better than other prediction models in the reported literature. In addition, an examination of the immunological surroundings indicates that the group with low risk exhibited elevated ESTIMATE score, ImmuneScores, and StromalScores. More, significant differences in infiltrating immune cells and the expression levels of immune-related genes were found between the two groups. In HCC patients, the PRG signature exhibits potential as a biomarker, offering a significant point of reference for tailoring individual therapy.

Keywords PANoptosis · Hepatocellular carcinoma · Immune microenvironment · Immunotherapy · Prognosis

Introduction

Hepatocellular carcinoma (HCC), a highly malignant tumor worldwide, is responsible for most instances of primary liver cancer [1]. Even though notable advances in HCC treatment were made, the overall prognosis of treated HCC- individuals still remains unfavorable [2, 3]. According to extensive investigations, it has been conducted in previous studies the development of a prognostic model for liver cancer by the comprehensive research institute of bioinformatics, including HCC [4, 5]. Nevertheless, the prognosis assessment, personalized diagnosis, and treatment for patients who were diagnosed with HCC continue to pose a considerable obstacle, primarily due to the insufficient exploration and practical application of prognostic tumor markers and therapeutic targets in research and clinical settings.

Cell death is an essential process to maintain normal functions of tissues and organisms [6]. When cells are seriously damaged, the function and structure of cells will

Xiaowu Wang and Liangchen Qu contributed equally to this work.

✉ Yangyang Guo
yang984054863@163.com

✉ Xingcheng Lin
linxingcheng86@163.com

1 The Third Affiliated Hospital of Wenzhou Medical University, Zhejiang Province, Rui'an 325200, China

2 Taizhou Hospital of Zhejiang Province Affiliated to Wenzhou Medical University, Taizhou 318000, Zhejiang Province, China

3 Wenzhou Medical University, Wenzhou 325000, Zhejiang Province, China

4 The First Affiliated Hospital of Ningbo University, Ningbo 315000, Zhejiang Province, China

Published online: 13 February 2025

undergo irreversible changes, that is, cell death [7]. To be specific, the categorization of cell death can be determined by the degree of control exerted over the process, resulting in uncontrollable accidental cell death (ACD) and controllable regulated cell death [8]. Regulated cell death is also known as programmed cell death (PCD) under normal physiological conditions, with pyroptosis, apoptosis, and necroptosis being the most thoroughly researched types of PCD [9]. The PCD processes include complicated molecular pathways that are involved in the initiation, transmission, and execution of cellular death [10, 11]. PANoptosis, a recently discovered cellular death process, comprises the interaction and synchronization of pyroptosis, apoptosis, and necroptosis [12, 13]. PANoptosis-related models have been studied in some cancers [14, 15]. Nonetheless, there is a major vacuum in understanding the influence of PRG on the prognosis and immunological landscape of HCC due to a lack of thorough study by academics throughout the world.

The objective of this research was to utilize molecular clustering and prognostic characteristics of PANoptosis in order to forecast the prognosis and effectiveness of immunotherapy in patients diagnosed with HCC. Initially, according to the expression levels of PRG in HCC patients, the people were grouped into two discrete PRG clusters. After identifying differentially expressed genes (DEGs) from the two PRG clusters, a prognosis model was established to classify these patients into high-risk and low-risk groups. This division facilitated the prediction of overall survival (OS) and immune response in the groups mentioned above.

Materials and methods

Data acquisition

At first, the TCGA-LIHC dataset from TCGA (https://portal.gdc.cancer.gov) was used to analyze 370 HCC tumor specimens and 53 control specimens for gene expression (measured in FPKM fragments per kilobase million). The corresponding clinical information was also included. Next, the above dataset was split into two groups to set up a training and testing division (ratio of 1:1), utilizing the R program (refer to Supplementary Table S1). In addition, validation was performed externally using 232 HCC tumor samples and their associated prognosis data, acquired from LIRI-JP of ICGC (https://dcc.icgc.org/). In addition, the investigation identified a combined number of 19 genes linked to PANoptosis, known as PRG, which were listed in Supplementary Table S2 [16]. The flowchart of this study is shown in Fig. 1.

PRG consensus clustering analysis

The R program "survival" was then used to analyze the connections between the identified clusters and OS. In this investigation, the R program packages "pheatmap," "survival," and "survminer" were applied to generate heat maps and the Kaplan–Meier (KM) curves to display the findings of the preceding analysis [17]. The DEG analysis between two clusters in this investigation was also done in the second alignment, based on utilizing the "limma" package [18] for DEG analysis throughout many studies, and the criteria utilized for defining DEGs were a |log fold change (FC)|> 1 and a false discovery rate (FDR) < 0.05. Finally, the CIBERSORT algorithm was used to determine the existence of invasion of immune cells, and differences in immune cell infiltration between the two subcategories were investigated.

Construction and validation of the PANoptosis-related prognostic signature

With the aim of identifying prognostic-related DEGs, a univariate Cox regression analysis was applied. Following this, a prognostic signature was developed by incorporating six DEGs, which were determined through least absolute shrinkage and selection operator (LASSO) regression analysis and multivariate Cox regression analysis. After the above process, sick persons with HCC were divided into low-risk and high-risk groups based on the median risk score. What's more, the OS was compared between the low-risk and high-risk groups by using KM analysis. Also, the "survival," "survminer," and "timeROC" R packages were performed in a bid to examine the OS and the receiver operating characteristic (ROC) of subgroups for durations of 1, 3, and 5 years. Principal component analysis (PCA) was implemented through the use of the "ggplot2" R package. Moreover, clinical factors and risk scores were integrated in order to establish a nomogram model. Lastly, multifactor ROC analyses and calibration graphs were performed to evaluate the prediction accuracy of the nomogram [19, 20].

Comparative analysis of the tumor microenvironment in the high- and low-risk groups

The ESTIMATE method was used to calculate the percentage of immune cells (ImmuneScores) and stromal cells (StromalScores). The XCELL, TIMER, QUANTISEQ, MCPCOUNTER, EPIC, CIBERSORT-ABS, and CIBERSORT algorithms were then adopted to assess the difference in immune cell infiltration between the high- and low-risk groups. Furthermore, the study chose the single sample gene set enrichment analysis (ssGSEA) technique

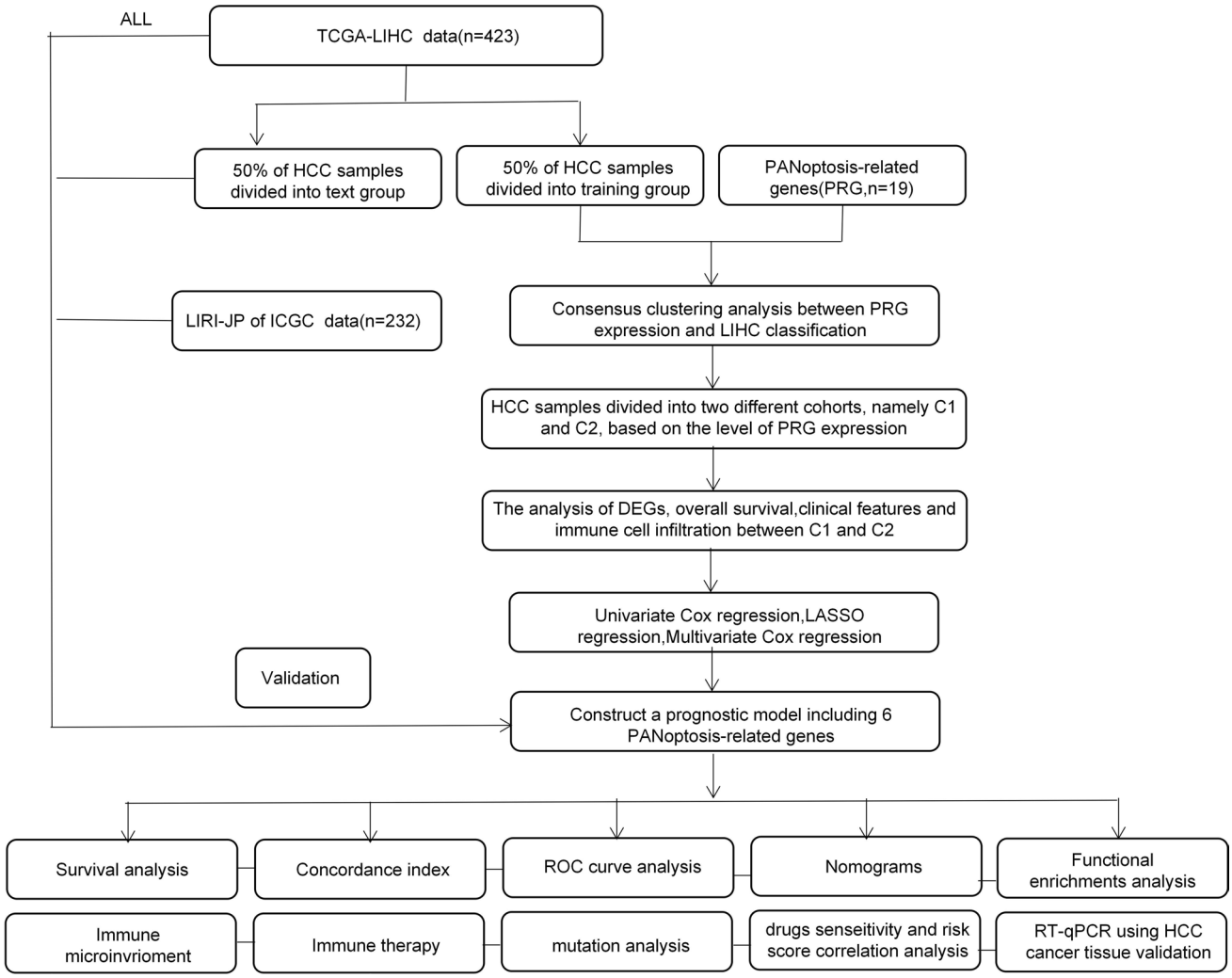

Fig. 1 The flowchart of this study

to compare immune cell infiltration and immunological function between the two groups. Also, the levels of genetic expression for immune-related genes were calculated. Tumor immune dysfunction and exclusion (TIDE) has emerged as a critical indicator for assessing immunotherapy effectiveness. In addition, an investigation was conducted to explore the relationship between the TIDE score and the risk score.

Pathway functional enrichment analysis of the PRG signature

Based on the DEGs identified (high-risk vs. low-risk groups, TCGA-LIHC data sets), "Gene Ontology" (GO) and "Kyoto Encyclopaedia of Genes and Genomes" (KEGG) analyses were carried out to refine the possible pathway analysis for these DEGs [21]. As well, "Genomic Variation Analysis" (GSVA) was done to investigate possible alterations in biological functioning between high-risk and low-risk patients.

Drug senseitivity analysis

The objective of this section was to examine the prognostic value of PRG signature in relation to the effectiveness of chemotherapy and targeted therapy medications. So we employed the "pRRophetic" algorithm to ascertain the half-maximal inhibitory concentration (IC_{50}) in common drugs, a measure of how well it modulated a specific biological or biological process [22].

Reverse transcription quantitative polymerase chain reaction (RT-qPCR)

Liver cancer patients' liver tissue samples were obtained from Ningbo First Hospital. Initially, we isolated total RNA using Trizol reagent (Thermofisher, USA) and performed reverse transcription to convert it into cDNA. Subsequently, we utilized SYBR Green Real-Time PCR Master Mix Plus

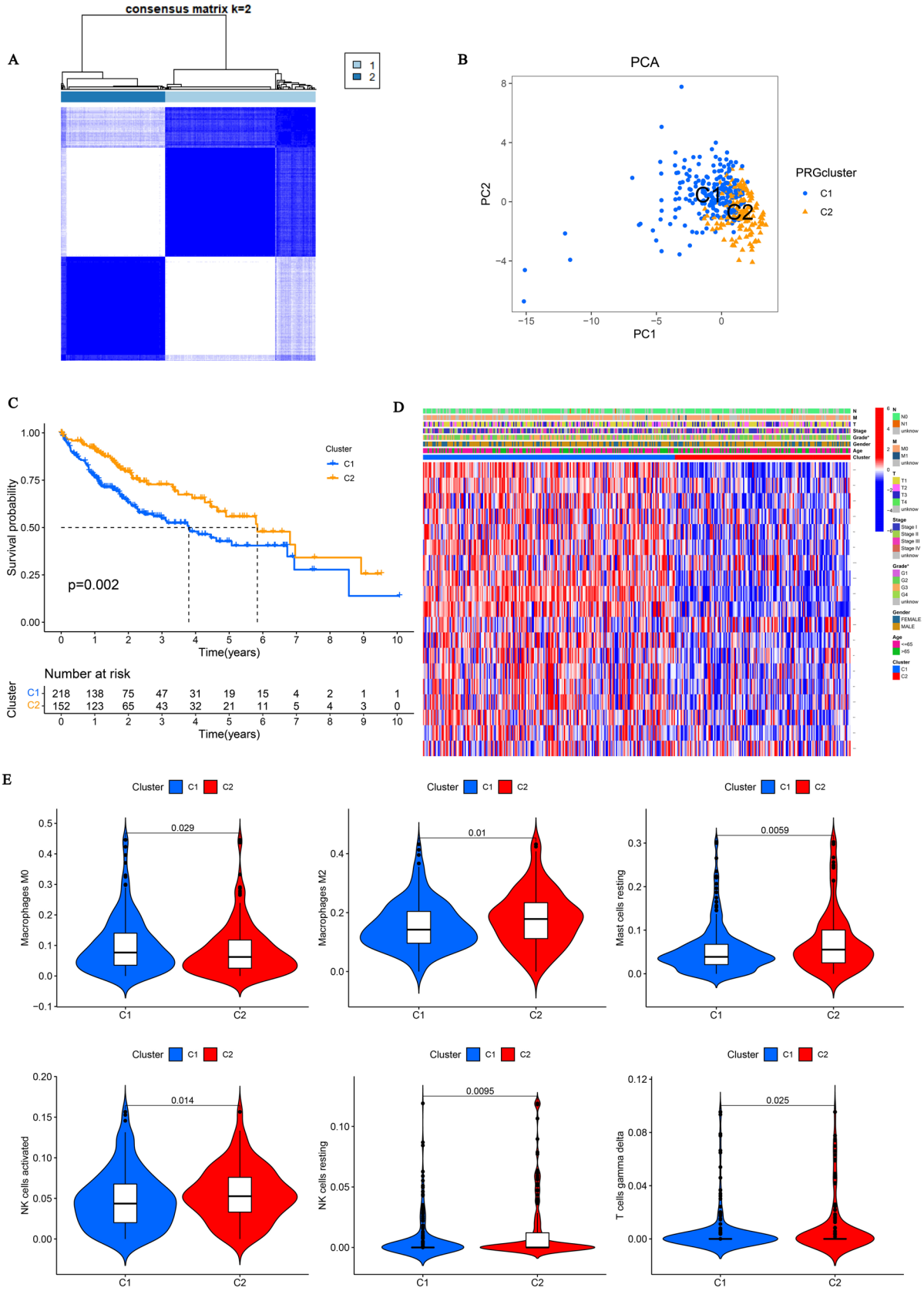
A
consensus matrix k=2
1
2
B
PCA
PC2
PC1
PRGcluster
C1
C2
C
Survival probability
p=0.002
Cluster
C1
C2
Time(years)
Number at risk
C1 218 138 75 47 31 19 15 4 2 1 1
C2 152 123 65 43 32 21 11 5 4 3 0
D
E
Macrophages M0
0.029
Macrophages M2
0.01
Mast cells resting
0.0059
NK cells activated
0.014
NK cells resting
0.0095
T cells gamma delta
0.025

◂**Fig. 2** PRG clusters and clinical characteristics between HCC samples in two clusters. **A** Two PRG clusters were defined using consensus clustering analyses. **B** PCA showed a good distinction between the two PRG clusters. **C** KM curve indicated that PRG cluster 2 had a longer survival time than PRG cluster 1. **D** Heatmaps showed the relationship between PRG clusters and clinical features and PRG expression in HCC patients. **E** The differences in immune cell infiltration between two clusters

(Toyobo, Japan) to perform RT-qPCR, with the internal reference gene β-actin being used for normalization. The primer sequences for amplification are listed in Supplementary Table S3.

Statistical analysis

The data involved in this study are presented in the form of mean ± SEM. Significant differences were evaluated by performing statistical analysis using Prism software (v6.02) and R software. The statistical analyses were conducted under the mentioned conditions: (1) Student's *T*-test was used to analyze variables between the two groups, (2) the Kruskal–Wallis test was used to analyze variables with two or more groups, and (3) correlations were examined using the Kruskal–Wallis test and Wilcoxon rank sum test, and the correlation between the two groups of variables was assessed using the Spearman correlation coefficient. The definition of statistical significance was established when the value of P was less than 0.05.

Results

Identification of PRG clusters in HCC

The study began by implementing consensus clustering analysis to investigate the correlation between PRG expression and HCC classification. The results shown in Fig. 2A demonstrated that HCC patients could be divided into two different cohorts, namely, C1 and C2, based on the level of PRG expression. Additionally, the application of PCA showed a clear differentiation between PRG cluster 1 and cluster 2, as illustrated in Fig. 2B. Importantly, the C2 group of HCC patients exhibited a longer survival duration compared to the C1 group, as shown in Fig. 2C. Moreover, the relationship between PRG clusters and PRG expression in individuals diagnosed with HCC is depicted in Fig. 2D.

Given the significant impact of immune cells on the onset and progression of HCC, we proceeded to examine the disparities between the two clusters in immune cell infiltration. Cluster 2 displayed notably elevated levels of macrophages M2, as well as resting mast cells, activated NK cells, and resting NK cells in comparison to cluster 1. Conversely, cluster 2 displayed lower levels of macrophages M1 as well as T cells gamma delta when compared to cluster 1 (Fig. 2E).

PANoptosis-related prognostic signature construction and verification

By utilizing the "limma" package for analysis of DEGs, a total of 1058 DEGs were discovered among the aforementioned clusters, adhering to the criteria of |log fold change (FC)|> 1 and FDR < 0.05. Afterward, a unique analysis revealed 330 DEGs linked to the prognosis of HCC. To tackle the problem of overfitting, a LASSO analysis was conducted, leading to the development of a prognostic signature comprising six genes (*CYP26B1*, *CKAP2*, *SLAMF6*, *S100A9*, *IL7R*, and *TRIM54*).The risk score formula was computed as follows: risk score = [*CYP26B1* × (0.4789)] + [*CKAP2* × (0.7281)] + [*SLAMF6* × (−0.7394)] + [*S100A9* × (0.3302)] + [*IL7R* × (−0.3709)] + [*TRIM54* × (0.2218)]. Therefore, we verified the differential expression of these six genes between the HCC tumor tissue and the normal tissue adjacent to the HCC tumor (Supplementary Figure S1).

Patients diagnosed with HCC were divided into high- and low-risk groups based on the median risk score. Patients with elevated risk scores in Fig. 2A exhibited an increased probability of mortality. Furthermore, Fig. 3B demonstrates the expression of these six genes in the two risk categories, while Fig. 3C clearly shows the segregation of the two risk groups through PCA analysis. Furthermore, the analysis of KM results depicted in Fig. 3D revealed a notable disparity in survival outcomes among the two risk categories ($P < 0.001$), indicating that the low-risk group exhibited superior results compared to the high-risk group. In the meantime, in Fig. 3E, the evaluation of the PRG signature was conducted using the ROC curve, resulting in AUC values for the 1-, 3-, and 5-year time intervals (1-year: 0.826, 3-year: 0.865, and 5-year: 0.868).

Furthermore, the aforementioned findings were corroborated through the examination of the test dataset. KM analysis was applied to categorize all patients diagnosed with HCC in the test dataset into high-risk and low-risk groups. The low-risk group had a more favorable prognosis compared to the high-risk group in the TCGA-test, TCGA-all, and ICGC-LIRI-JP datasets, as indicated by the observations (Fig. 4A–C). Regarding the ROC in these datasets, the values for the area under the ROC curve for intervals of 1, 3, and 5 years in the TCGA-test dataset were 0.739, 0.679, and 0.709, respectively (as shown in Fig. 4D). Similarly, the AUC values for the same intervals in the TCGA-all dataset were 0.804, 0.784, and 0.716, respectively (as shown in Fig. 4E). Additionally, the AUC values for prognostic predictions of 1, 3, and 5 years in the ICGC-LIRI-JP dataset were found to be 0.734, 0.708,

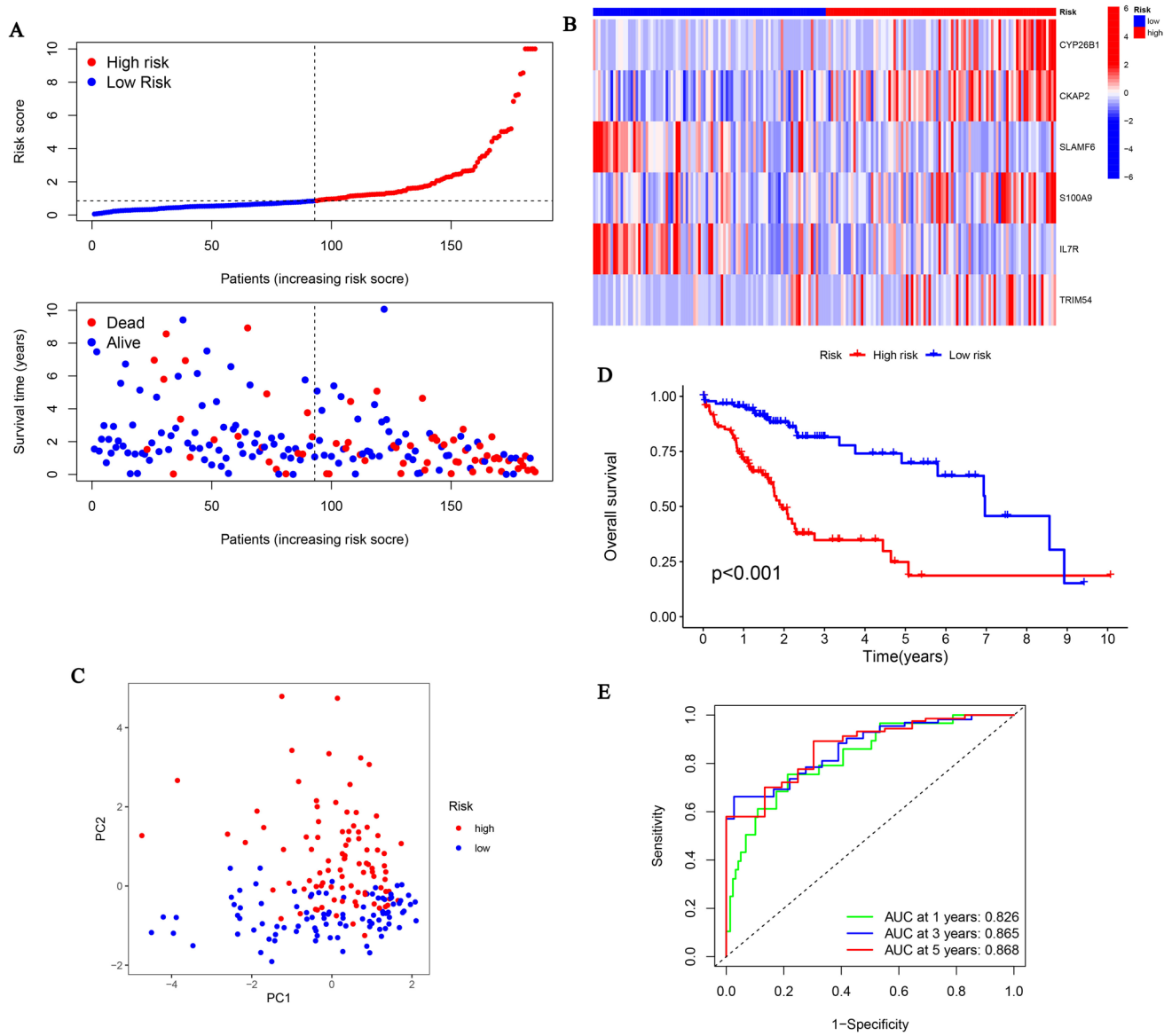

Fig. 3 Construction of the prognostic signature. **A** Risk score and survival outcome of each case. **B** Heatmap showed the expression of 6 genes in two risk groups. **C** PCA showed a good distinction between high-risk and low-risk. **D** The KM curve showed that patients in the high-risk group had a worse prognosis. **E** The AUC for 1-, 3-, and 5-years survival

and 0.868, respectively (as shown in Fig. 4F). Additionally, our PRG signature was evaluated in different clinical subgroups within the TCGA dataset for its prognostic predictive capability. The investigation revealed that the PRG signature had significant prognostic value in patients grouped by age (older than 65, $P < 0.001$; 65 or younger, $P < 0.001$), sex (female, $P = 0.008$; male, $P < 0.001$), tumor grade (G1-2, $P < 0.001$; G3-4, $P = 0.015$), metastasis status (M0, $P < 0.001$), lymph node involvement (N0, $P < 0.001$), tumor stage (stage I-II, $P < 0.001$; stage III-IV, $P = 0.006$), and tumor size (T1-2, $P < 0.001$; T3-4, $P = 0.006$), as shown in Fig. 5.

Nomogram construction

In comparison to prognosis models developed by previous researchers, our PRG signature exhibited a significantly higher C-index (Fig. 6A). By combining the PRG signature with clinical characteristics, we developed an innovative nomogram to enhance the predictive significance of the PRG signature as shown in Fig. 6B. The novel nomogram demonstrated strong prognostic predictive abilities according to the calibration curves (Fig. 6C). Additionally, we conducted ROC analysis to compare the prognostic predictive value of the nomogram with other individual factors, including gender, grade, risk, and age. In Fig. 6D,

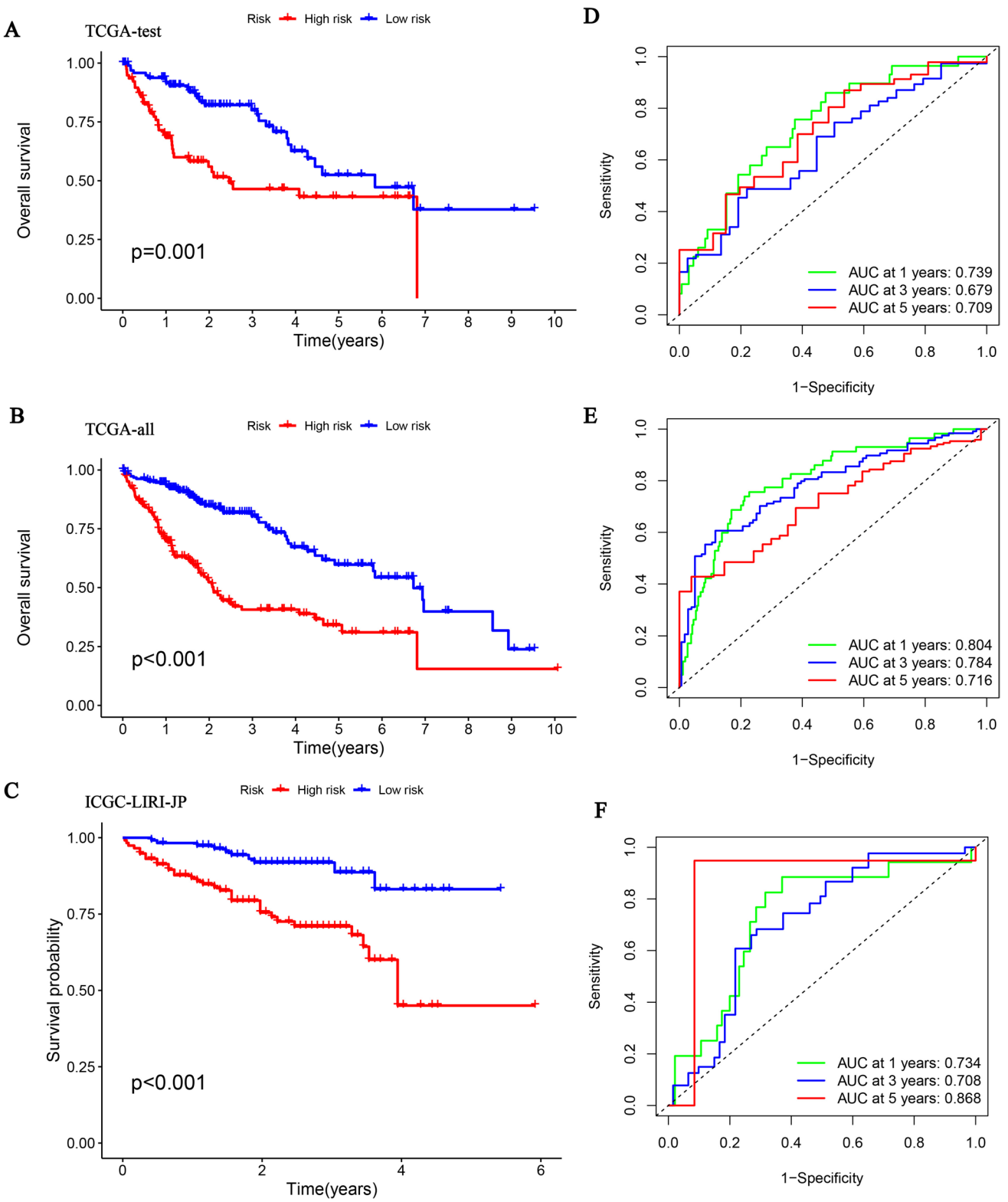

Fig. 4 Validation of the prognostic signature. KM curve showed that patients in the high-risk group had a worse prognosis in TCGA-test (**A**), TCGA-all (**B**), and ICGC-LIRI-JP (**C**). The AUC for 1-, 3-, and 5-years survival in TCGA-test (**D**), TCGA-all (**E**), and ICGC-LIRI-JP (**F**)

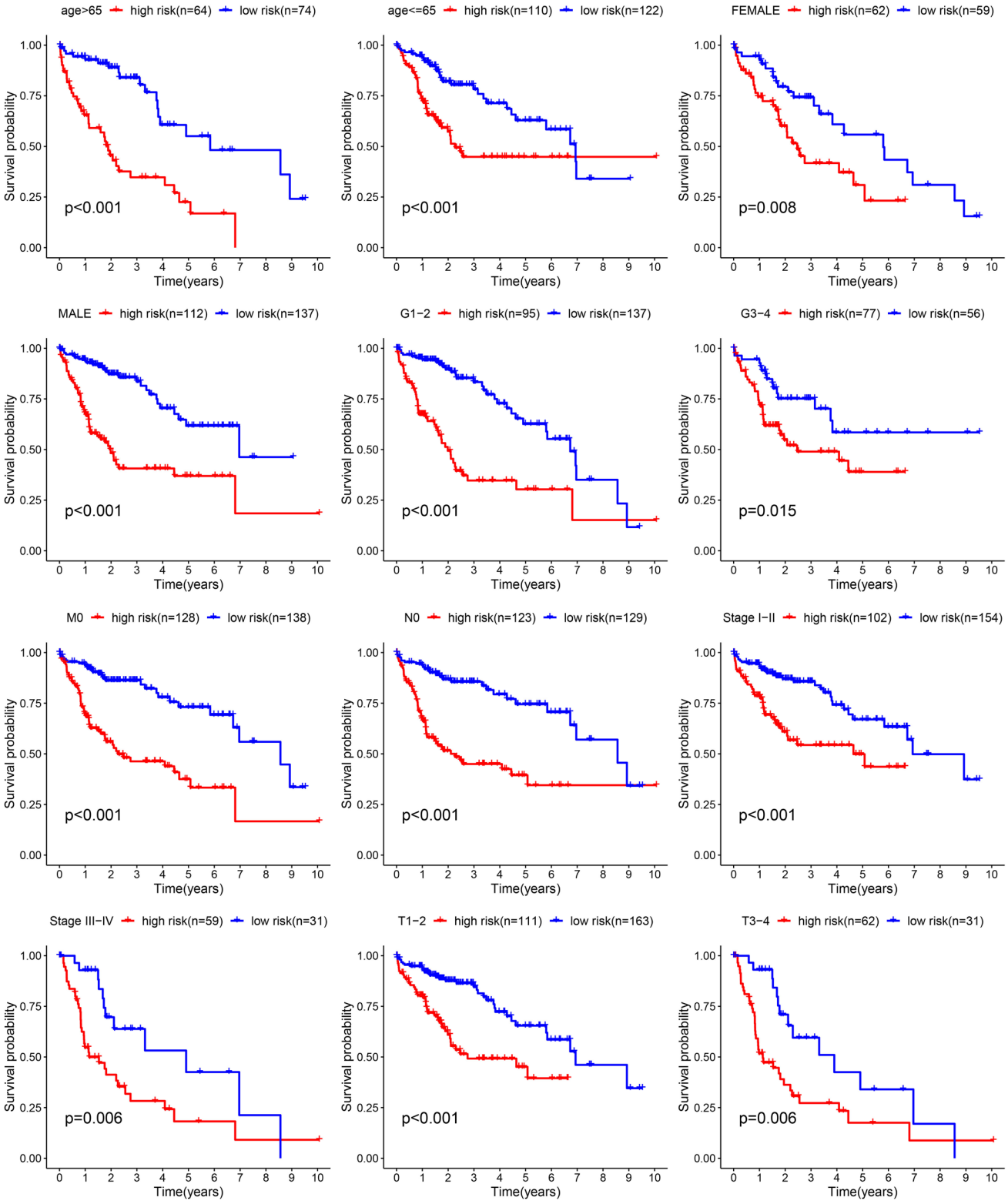

Fig. 5 Validation of the prognostic value of PRG signature in different clinical characteristics groups

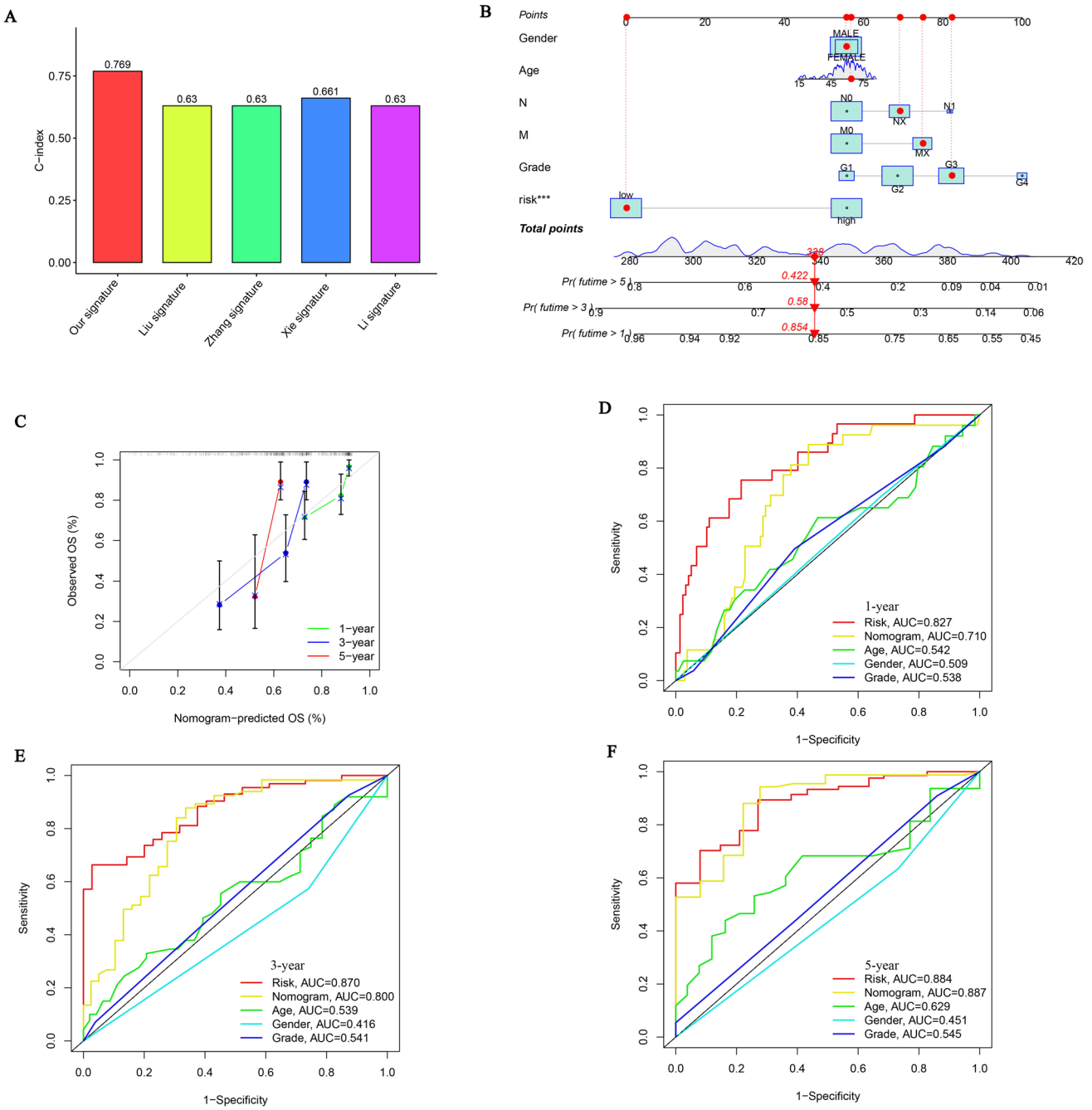

Fig. 6 Construction and assessment of nomogram. **A** C-index of different models. **B** The prediction of nomogram in the TCGA-train dataset. **C** Calibration plots for the nomogram. The multifactor AUC for 1- (**D**), 3- (**E**), and 5-years (**F**) survival

the nomogram and risk score had AUC values of 0.710 and 0.827, respectively, for 1-year survival times. In the same way, the AUC values for 3-year survival durations were 0.800 (using the nomogram) and 0.870 (with the risk score), as shown in Fig. 6E. In conclusion, the AUC values for 5-year survival times were 0.887 (nomogram) and 0.884 (risk score) as depicted in Fig. 6F. These findings indicate that the newly developed nomogram exhibits promising potential as a reliable prognostic prediction model.

Comparative assessment of the tumor microenvironments in groups with high and low risks

The tumor microenvironments exerted a substantial influence on the tumor's biological characteristics. Using the ESTIMATE algorithm, researchers noticed a significant decrease in the ImuneScores, StromalScores, and ESTIMATE scores in the high-risk group when compared to the low-risk group (Fig. 7A). Moreover, diverse computational methods including XCELL, TIMER, QUANTISEQ, MCPCOUNTER, EPIC, CIBERSORT-ABS, and CIBERSORT were employed to examine the levels of immune cells in both high-risk and low-risk groups. According to the results, the low-risk groups showed elevated levels of immune cells, as indicated in Fig. 7B. The

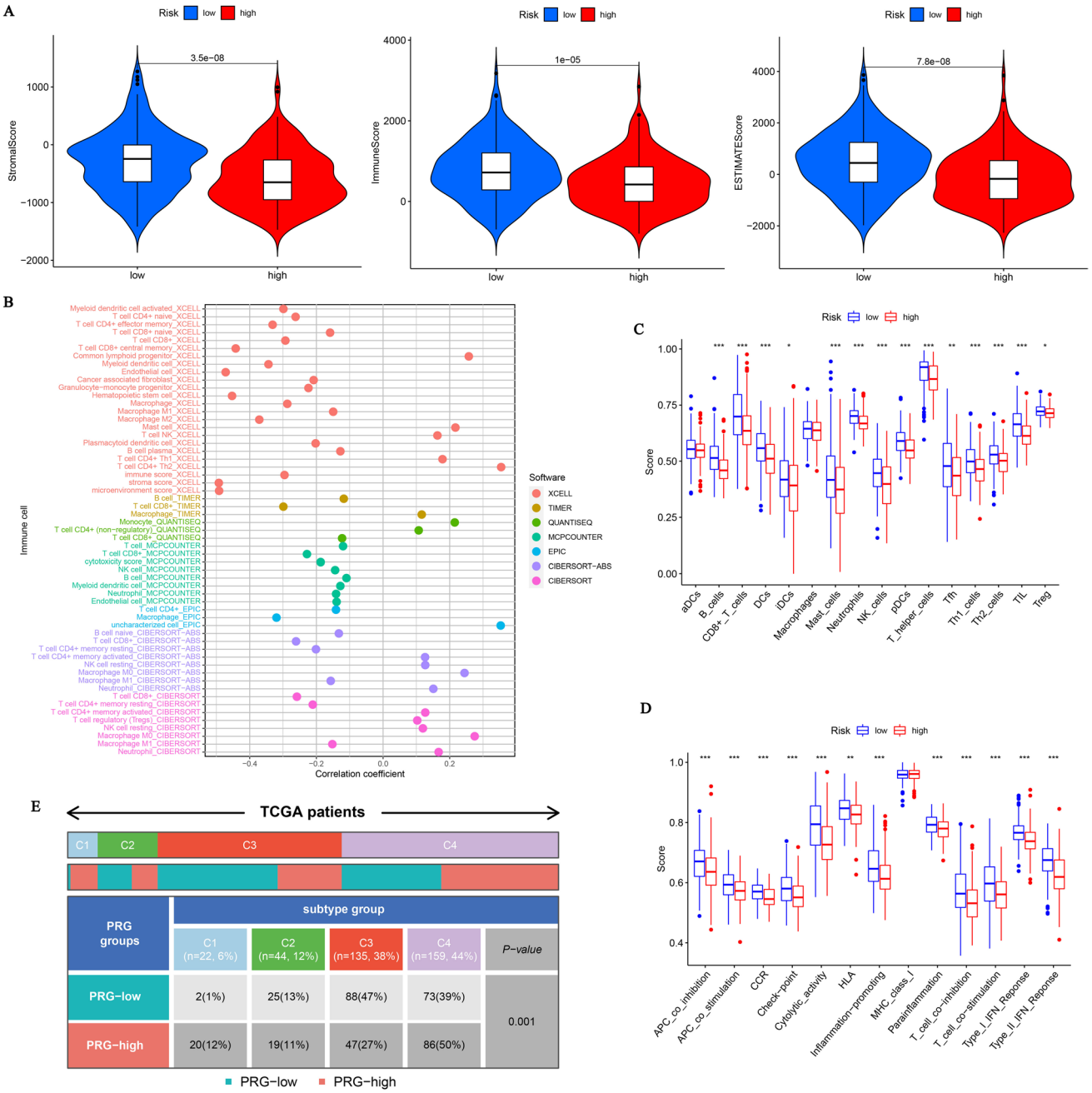

Fig. 7 Analysis of immune conditions of high- and low-risk groups. **A** Differences in immune microenvironment scores between the two groups. **B** The analysis of differences in immune cell infiltration between the two groups with multiple algorithms. **C** The analysis of differences in immune cell infiltration between the two groups with ssGSEA. **D** The analysis of differences in immune functions between the two groups with ssGSEA. **E** The distribution of patients with high- and low-risk in different immune subtypes

low-risk group may potentially have a more positive outlook linked to this observation. In addition, the ssGSEA analysis showed that different types of immune cells, such as B lymphocytes, CD8 + T lymphocytes, dendritic cells (DCs), iDCs, mast cells, neutrophils, NK cells, pDCs, T helper cells, Tfh, Th1 cells, Th2 cells, tumor-infiltrating lymphocyte (TIL), and T cells regulatory (Treg), had decreased levels of infiltration in high-risk patients when compared to low-risk patients (Fig. 7C). Additionally, the low-risk patients demonstrated improved immunologic function across multiple measures (Fig. 7D). As well, Fig. 7E portrays the distribution of high-risk versus low-risk patients categorized within various immune subtypes.

To proceed further, we compared the levels of immune-related gene expressions in the high-risk and low-risk groups. In comparison to individuals with low risk, those at high risk showed a significant reduction in the expression of genes related to immune function (Fig. 8A–D). Besides, the TIDE score had emerged as a noteworthy biomarker for prognosticating the effectiveness of immunotherapy. As a result, an investigation into the relationship between TIDE scores and risk scores was launched. Figure 8E reveals a notable difference in TIDE scores between the low-risk

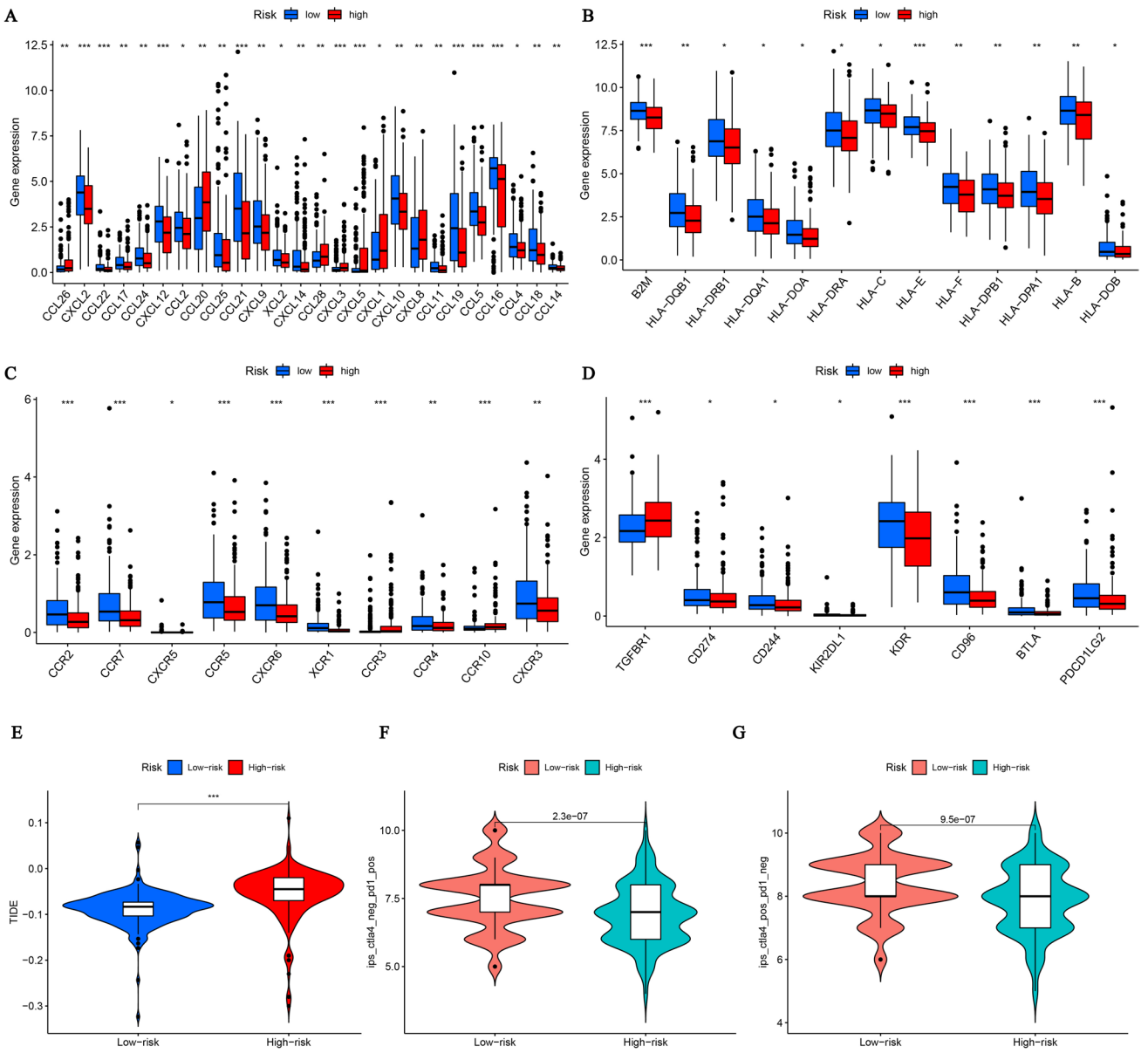

Fig. 8 Assessment of Immunotherapy response of high- and low-risk groups. **A**–**D** The immune-related gene expression levels in different groups. **E** Relationship between TMB score and risk score. **F** Relationship between MSI score and risk score. **G** The TIDE scores in different groups

and high-risk groups, suggesting that patients classified as low-risk might experience a more favorable reaction to immunotherapy. Furthermore, the immunophenotype score of individuals in the low-risk category displayed a predominantly elevated level compared to that of individuals in the high-risk category (as shown in Fig. 8F and G). These findings strongly indicate that patients categorized as low-risk may potentially demonstrate a superior response to immunotherapy in contrast to those classified as high-risk.

Examining mutations and assessing the functional significance of the PRG signature through comparative analysis

For the purpose of enhancing the understanding of the pathobiological relevance of the PRG score, a comparison of somatic mutations was conducted between HCC cases with high and low PRG scores. The results showed that somatic mutations were more prevalent in the high-PRG-score group (89.35%) than in the low-PRG-score group (82.29%) (Fig. 9A, B). An analysis of both GO and KEGG data was then conducted for the genes that showed differential expression to determine their potential biological functions. According to the GO analysis, the DEGs showed significant enrichment in antigen binding, immunoglobulin complex, and binding to immunoglobulin receptors (Fig. 9C). Furthermore, the KEGG analysis revealed a significant enrichment of the distinct genes in both the cell cycle and the p53 signaling pathway (Fig. 9D). Moreover, GSVA unveiled substantial alterations in numerous pathways among the high-risk group (Fig. 9E).

The drug sensitivity and risk score correlation analysis

We conducted an analysis to examine the difference in drug sensitivity between HCC patients at high risk and low risk. In this analysis, we correlated the risk scores of HCC patients with the IC_{50} values of chemotherapy and targeted therapy drugs. The results of this research indicated that the IC_{50} values for six medications (AMG-706, AKT inhibitor VIII, EKB-569, GSK2126458, HG-6–64-1, IPA-3) were significantly reduced in the high-risk category. In contrast, the high-risk group exhibited higher IC_{50} values for CI-1040, DMOG, and MP470 (Fig. 10).

Discussion

HCC is the most common type of primary liver cancer. Its treatment mainly involves surgical procedures, along with interventional therapy, radiotherapy, chemotherapy, targeted medications, and immunotherapy [23, 24]. Despite the presence of multiple treatment options, patients with HCC continue to have a bleak outlook due to factors like the return of the disease and its spread to other parts of the body. PANoptosis, a recently identified cell death pathway, encompasses the interplay and synchronization of pyroptosis, apoptosis, and necroptosis [12]. In spite of this, there is still an obvious gap in how PRG may impact HCC prognosis and immune landscape.

In recent decades, the advent of high-throughput sequencing technology and the availability of public databases have enabled the quantitative detection of molecular prognostic markers, facilitating the prediction of tumor progression [25, 26]. Studies have demonstrated that prognostic models possess distinct advantages in forecasting the prognosis of HCC patients [27, 28]. Hence, providing guidance for clinical decision-making would be beneficial by constructing and validating a prognosis model of PRG to assess a patient's prognosis after being diagnosed with HCC using multiple datasets.

In this study, we obtained the HCC-related datasets from TCGA and the ICGC and subsequently partitioned TCGA-LIHC into a training group as well as a testing group using random allocation. As part of our endeavor to discover a predictive signature, consisting of six genes, we conducted a univariate Cox regression and LASSO analysis using the TCGA-training dataset. The evaluation of the PRG signature prognosis was conducted on the TCGA-test, TCGA-all, and ICGC-LIRI-JP datasets. In order to enhance PRG's signature functionality, a novel nomogram was developed, incorporating both clinicopathological features and the risk score of HCC patients. The calibration curve demonstrated a strong linear fit, indicating the predictive capability of our nomogram for prognosis assessment.

The created PRG signature showed a significant association with the prognosis of patients with HCC. The signature consisted of six genes, specifically *CYP26B1*, *CKAP2*, *SLAMF6*, *S100A9*, *IL7R*, and *TRIM54*, that had been widely associated with different forms of cancer. Chen et al. [29] discovered a novel involvement of the *CYP26B1* gene in the pathogenesis of oral squamous cell carcinoma induced by betel quid consumption. By activating FAK-ERK2, CKAP2 assisted cervical cancer cells in proliferating and metastasizing, according to Guo et al. [30]. In their study, Yigit and colleagues [31] showed that *SLAMF6* functions as a controller for exhausted $CD8^+$ T cells in cancer. It had been shown that activation of the *S100A9-CXCL12* signal axis contributed to the development of an immunosuppressive microenvironment in *BRCA1*-mutated breast cancer, which had been linked to resistance against immunotherapy medications [32]. In esophageal squamous cell carcinoma, Kim et al. [33] provided evidence indicating that the histone deacetylase inhibitor suppressed the oncogenic *IL7R* by regulating

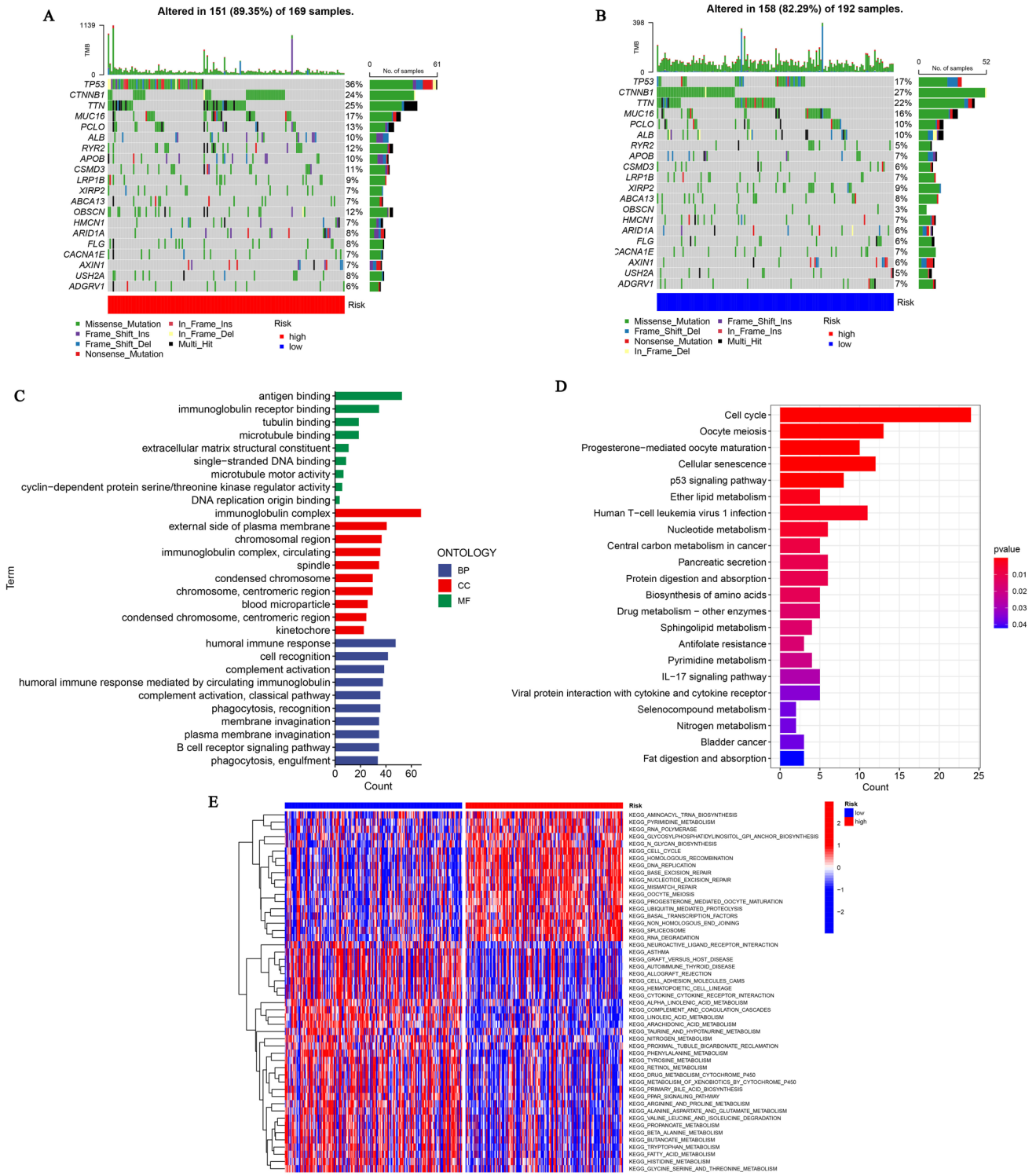

Fig. 9 Function analysis. The somatic gene mutations in high-risk group (**A**) and low-risk group (**B**). **C** GO analysis of differential genes between high- and low-risk groups. **D** KEGG analysis of differential genes between high- and low-risk groups. **E** GSVA enrichment analysis in high- and low-risk groups

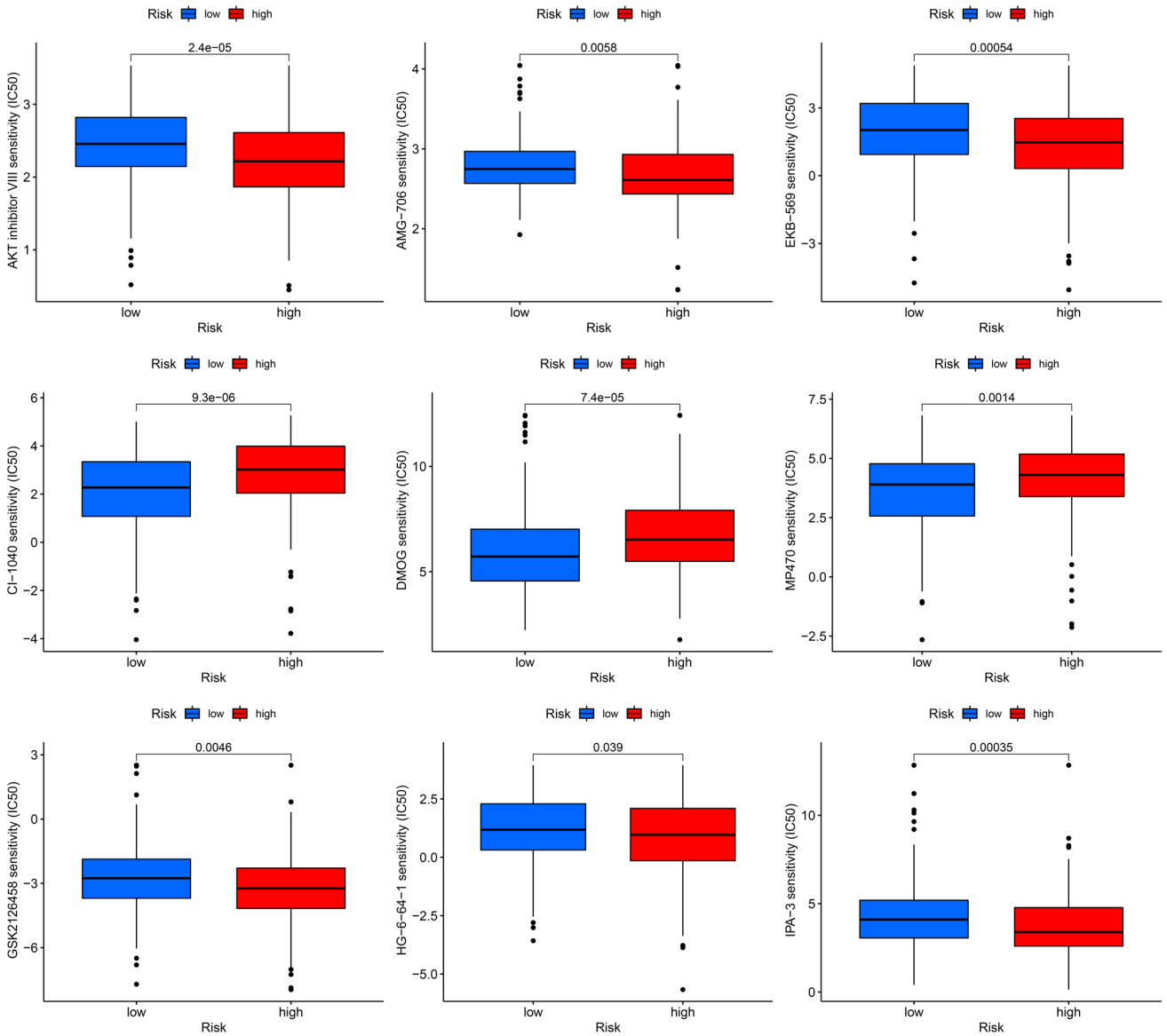

Fig. 10 Drug sensitivity analysis in high- and low-risk groups

acetylated *FOXO1*. However, the level of contribution of these genes to HCC remained insufficiently understood.

The tumor microenvironment (TME) consisted of a diverse collection of immune cells, interstitial cells, components of the extracellular matrix, and tumor vasculature, all of which played a vital role in the onset and progression of the tumor [34]. The levels of infiltrating immune cells within the TME typically undergo alterations during tumorigenesis and disease progression [35]. In our investigation, patients with low-risk scores exhibited elevated ImuneScores, StromalScores, and ESTIMATEScores. The high-risk group exhibited a notable reduction in the abundance of several immune cell types (including B cells, CD8 + T cells, dendritic cells, iDCs, mast cells, neutrophils, NK cells, pDCs, T helper cells, Tfh, Th1 cells, Th2 cells, tumor-infiltrating lymphocyte, and T cells regulatory) when compared to the low-risk group. Furthermore, the patients with low risk demonstrated enhanced immune function and a propensity for reduced expression of genes associated with the immune system compared to the high-risk group. It is also widely recognized that immune cells played an important part in anti-tumor immunity. Therefore, there was a possibility that the diminished number and functionality of immune cells contribute to the unfavorable prognosis observed in patients with high-risk diseases. The TIDE score played a vital role as a marker for the response to immunotherapy [36, 37]. Our study showed that the TIDE score was notably reduced in the low-risk category in comparison to the high-risk category. The results suggested that HCC

patients classified as low-risk may demonstrate a heightened reaction to immunotherapy compared to those categorized as high-risk. Furthermore, the study's practical implications also encompassed providing guidance for the clinical implementation of immunotherapy and chemotherapy in patients with HCC, leading to a deeper comprehension of the involvement of PANoptosis in HCC.

The primary basis for our analyses was derived from publicly accessible datasets, with all samples obtained retrospectively, thereby potentially introducing inherent case selection bias. Moreover, it was crucial to conduct additional in vitro and in vivo experiments in order to validate our research findings.

In summary, we had successfully developed a molecular cluster and prognostic signature utilizing PANoptosis, which held significant implications for survival prediction, immunotherapy, and clinical treatment guidance. The findings of this investigation had the potential to enhance our comprehension of PANoptosis in HCC and facilitate the development of more efficacious treatment approaches. Despite these limitations, it was essential to acknowledge them, and additional experiments were warranted to validate our research outcomes.

Supplementary Information The online version contains supplementary material available at https://doi.org/10.1007/s12026-025-09603-y.

Acknowledgements We would like to extend our heartfelt appreciation to the GEO and TCGA databases for their assistance in creating favorable research conditions and offering invaluable data resources.

Author contribution W.X. and Q.L., investigation (leading), formal analysis (leading), writing-original draft (leading), conceptualization, writing-review and editing, contributed equally; W.Z.K., W.Z.X., X.Y., Y.Z., and Y.X., investigation (participating), writing-original draft (participating), experiment (participating); G.Y. and L.X., conceptualization, writing-review and editing.

Data availability The datasets used and examined in this study can be obtained from the corresponding author upon a reasonable inquiry.

Declarations

Ethics approval All experimental protocols were approved by the ethics committee of Ningbo First Hospital (068A01) and were carried out in accordance with relevant guidelines and regulations.

Consent to participate Our research was in line with the Declaration of Helsinki. Written informed consent was obtained from all patients and/or their legal guardian(s) for the publication of this research.

Competing interest The authors declare no competing interests.

References

1. Rahimi-Farsi N, Bostanian F, Shahbazi T, Shamsinejad FS, Bolideei M, Mohseni P, Zangooie A, Boustani F, Shoorei H. Novel oncogenes and tumor suppressor genes in hepatocellular carcinoma: carcinogenesis, progression, and therapeutic targets. Gene. 2025;10:149229.
2. Cersosimo RJ. Systemic targeted and immunotherapy for advanced hepatocellular carcinoma. Am J Health Syst Pharm. 2021;78(3):187–202.
3. Li B, Cao Y, Meng G, Qian L, Xu T, Yan C, Luo O, Wang S, Wei J, Ding Y, et al. Targeting glutaminase 1 attenuates stemness properties in hepatocellular carcinoma by increasing reactive oxygen species and suppressing Wnt/beta-catenin pathway. EBioMedicine. 2019;39:239–54.
4. Tang X, Ren X, Huang T, Miao Y, Ha W, Li Z, Yang L, Mi D. Prognostic and immunological significance of the molecular subtypes and risk signatures based on cuproptosis in hepatocellular carcinoma. Mediators Inflamm. 2023;20(2023):3951940.
5. Chi H, Zhao S, Yang J, Gao X, Peng G, Zhang J, Xie X, Song G, Xu K, Xia Z, Chen S, Zhao J. T-cell exhaustion signatures characterize the immune landscape and predict HCC prognosis via integrating single-cell RNA-seq and bulk RNA-sequencing. Front Immunol. 2023;15(14):1137025.
6. Vanden Berghe T, Linkermann A, Jouan-Lanhouet S, Walczak H, Vandenabeele P. Regulated necrosis: the expanding network of non-apoptotic cell death pathways. Nat Rev Mol Cell Biol. 2014;15:135–47.
7. Green DR, Llambi F: Cell death signaling. Cold Spring Harb Perspect Biol 2015;7(12).
8. Wang Y, Kanneganti TD. From pyroptosis, apoptosis and necroptosis to PANoptosis: a mechanistic compendium of programmed cell death pathways. Comput Struct Biotechnol J. 2021;3(19):4641–57.
9. Liu J, Hong M, Li Y, Chen D, Wu Y, Hu Y. Programmed cell death tunes tumor immunity. Front Immunol. 2022;13:847345.
10. Chi H, Chang HY, Sang TK. Neuronal cell death mechanisms in major neurodegenerative diseases. Int J Mol Sci 2018, 19(10).
11. Shi X, Han S, Wang G, Zhou G. Mitochondrial-associated programmed-cell-death patterns for predicting the prognosis of non-small-cell lung cancer. Front Med. 2024.
12. Wang Y, Kanneganti TD. From pyroptosis, apoptosis and necroptosis to PANoptosis: a mechanistic compendium of programmed cell death pathways. Comput Struct Biotechnol J. 2021;19:4641–57.
13. Christgen S, Zheng M, Kesavardhana S, Karki R, Malireddi RKS, Banoth B, Place DE, Briard B, Sharma BR, Tuladhar S, et al. Identification of the PANoptosome: a molecular platform triggering pyroptosis, apoptosis, and necroptosis (PANoptosis). Front Cell Infect Microbiol. 2020;10:237.
14. Bao L, Ye Y, Zhang X, Xu X, Wang W, Jiang B. Identification and verification of a PANoptosis-related long noncoding ribonucleic acid signature for predicting the clinical outcomes and immune landscape in lung adenocarcinoma. Heliyon. 2024;10(8):e29869.
15. Zhao Q, Ye Y, Zhang Q, Wu Y, Wang G, Gui Z, Zhang M. PANoptosis-related long non-coding RNA signature to predict the

prognosis and immune landscapes of pancreatic adenocarcinoma. Biochem Biophys Rep. 2023;7(37):101600.
16. Wang X, Sun R, Chan S, Meng L, Xu Y, Zuo X, Wang Z, Hu X, Han Q, Dai L, et al. PANoptosis-based molecular clustering and prognostic signature predicts patient survival and immune landscape in colon cancer. Front Genet. 2022;13:955355.
17. Wu T, Hu E, Xu S, Chen M, Guo P, Dai Z, et al. clusterProfiler 4.0: a universal enrichment tool for interpreting omics data. Innovation (Cambridge (Mass)). 2021;2:100141.
18. Ritchie ME, Phipson B, Wu D, et al. limma powers differential expression analyses for RNA-sequencing and microarray studies. Nucleic Acids Res. 2015;43:e47.
19. Yu G, Wang LG, Han Y, He QY. clusterProfiler: an r package for comparing biological themes among gene clusters. Omics J Integr Biol. 2012;16(5):284–7.
20. Li J, Qiao H, Wu F, Sun S, Feng C, Li C, Yan W, Lv W, Wu H, Liu M, et al. A novel hypoxia- and lactate metabolism-related signature to predict prognosis and immunotherapy responses for breast cancer by integrating machine learning and bioinformatic analyses. Front Immunol. 2022;13:998140.
21. Zhao Y, Zhang Y, Dai C, Hong K, Guo Y. A signature constructed with mitophagy-related genes to predict the prognosis and therapy response for breast cancer. Aging (Albany NY). 2022;14(15):6169–86.
22. Bai Y, Zhang Q, Liu F, Quan J. A novel cuproptosis-related lncRNA signature predicts the prognosis and immune landscape in bladder cancer. Front Immunol. 2022;13:1027449.
23. Huang L, Liu R, Zhou P, Tian Y, Lu Z: miR-9 and miR-181a target Gab2 to inhibit the proliferation and migration of hepatocellular carcinoma HepG2 cells. Genes (Basel) 2022;13(11).
24. Lu YF, Zhou JP, Zhou QM, Yang XY, Wang XJ, Yu JN, Zhang JG, Du YZ, Yu RS. Ultra-thin layered double hydroxide-mediated photothermal therapy combine with asynchronous blockade of PD-L1 and NR2F6 inhibit hepatocellular carcinoma. J Nanobiotechnology. 2022;20(1):351.
25. Zeng R, Li Y, He DM, Sun MZ, Huang WQ, Wang YH, Zhuo YM, Chen JJ, Chen TH, Guo JH, et al. Potassium channel-related genes are a novel prognostic signature for the tumor microenvironment of renal clear cell carcinoma. Front Oncol. 2022;12:1013324.
26. Tian XM, Xiang B, Jin LM, Mi T, Wang JK, Zhanghuang C, Zhang ZX, Chen ML, Shi QL, Liu F, et al. Immune-related gene signature associates with immune landscape and predicts prognosis accurately in patients with Wilms tumour. Front Immunol. 2022;13:920666.
27. Gao Z, Chen J, Zhou Y, Deng P, Sun L, Qi J, Zhang P. A novel metabolism-related gene signature for predicting the prognosis of HBV-infected hepatocellular carcinoma. J Oncol. 2022;2022:2391265.
28. Yu L, Liu X, Wang X, Yan H, Pu Q, Xie Y, Du J, Yang Z. Glycometabolism-related gene signature of hepatocellular carcinoma predicts prognosis and guides immunotherapy. Front Cell Dev Biol. 2022;10:940551.
29. Chen PH, Lee KW, Chen CH, Shieh TY, Ho PS, Wang SJ, Lee CH, Yang SF, Chen MK, Chiang SL, et al. CYP26B1 is a novel candidate gene for betel quid-related oral squamous cell carcinoma. Oral Oncol. 2011;47(7):594–600.
30. Guo QS, Song Y, Hua KQ, Gao SJ. Involvement of FAK-ERK2 signaling pathway in CKAP2-induced proliferation and motility in cervical carcinoma cell lines. Sci Rep. 2017;7(1):2117.
31. Yigit B, Wang N, Ten Hacken E, Chen SS, Bhan AK, Suarez-Fueyo A, Katsuyama E, Tsokos GC, Chiorazzi N, Wu CJ, et al. SLAMF6 as a regulator of exhausted CD8(+) T cells in cancer. Cancer Immunol Res. 2019;7(9):1485–96.
32. Li J, Shu X, Xu J, Su SM, Chan UI, Mo L, Liu J, Zhang X, Adhav R, Chen Q, et al. S100A9-CXCL12 activation in BRCA1-mutant breast cancer promotes an immunosuppressive microenvironment associated with resistance to immunotherapy. Nat Commun. 2022;13(1):1481.
33. Kim MJ, Choi SK, Hong SH, Eun JW, Nam SW, Han JW, You JS. Oncogenic IL7R is downregulated by histone deacetylase inhibitor in esophageal squamous cell carcinoma via modulation of acetylated FOXO1. Int J Oncol. 2018;53(1):395–403.
34. Li T, Liu R, Zhang G, Jia Y, Pan L, Li Y, Jia C. Pan-cancer analysis of TLE3 revealed its value in tumor microenvironment and prognosis. J Oncol. 2022;2022:4085770.
35. Dong S, Hou D, Peng Y, Chen X, Li H, Wang H: Pan-cancer analysis of the prognostic and immunotherapeutic value of MITD1. Cells 2022;11(20).
36. Zhang C, Zhang Z, Sun N, Zhang Z, Zhang G, Wang F, Luo Y, Che Y, He J. Identification of a costimulatory molecule-based signature for predicting prognosis risk and immunotherapy response in patients with lung adenocarcinoma. Oncoimmunology. 2020;9(1):1824641.
37. Li X, Song D, Su S, He X, Cao F, Yang C, Li K, Huang S, Li C, Wang C, et al. Critical role of guanylate binding protein 5 in tumor immune microenvironment and predictive value of immunotherapy response. Front Genet. 2022;13:984615.